A Geometrical Linearization Approach for Salient-pole PMSM Optimal Voltage/Current Constrained Control over Whole Speed Range

Li Yang, Rui Gao, Wensong Yu, Iqbal Husain
FREEDM System Center
North Carolina State University
Email: lyang20,rgao,wyu2,ihusain2@ncsu.edu

***Abstract*—Permanent Magnet Synchronous Machine (PMSM) torque control over a wide speed range is essentially an optimization problem that treats torque error minimization as the objective function with inverter voltage and current as constraints. It is usually time consuming and difficult to solve such optimization problem for closed-form solutions since torque, voltage and current equations are all non-linear in the problem. In this paper, a model linearization based approach is proposed to manage the calculation complexity for such non-linear optimization. By dividing the problem into two sub-optimizations and solving them sequentially, the calculation is simplified. By identifying different operating regions of the PMSM, the closed-form solutions can be obtained geometrically with model linearization, which further simplifies the optimization process. The proposed algorithm is implemented for PMSM current loop controller design; simulation results show a good performance of the controller.**

***Index Terms*—optimization control, Permanent Magnet Synchronous Machine(PMSM), Maximum Torque per Amp(MTPA), Maximum Torque per Volt(MTPV).**

I. Introduction

Permanent Magnet Synchronous Machine (PMSM) torque control over the whole speed range requires identification of optimal current trajectory that maximizes torque output. The typical PMSM current trajectory on i_d-i_q plane can be divided into four regions[1], as shown in Fig.1. Region 1 is the Maximum Torque per Amp (MTPA) operation which generates the required torque with minimum phase current. Region 2 is when current trajectory moves away from MTPA curve along the torque hyperbola. Region 3 is when flux weakening operation begins and current trajectory moves along current limitation circle. Region 4 is the Maximum Torque per Volt (MTPV) operation which generates maximum torque possible under inverter voltage limitation.

Many research have been conducted towards PMSM torque control over whole speed range. In [2] an algorithm has been proposed for torque control in Regions 1 and 4. However, the proposed MTPA algorithm cannot perform well for accurate torque control since there is no explicit relationship between torque and phase current. In [3] a linearization based optimization approach has been proposed for Regions 1 - 3 control where the current references can be obtained based on torque command in MTPA operation; this allows accurate torque control but MTPV control is not possible since voltage constraint is over simplified. In [4]-[5], a Model Predictive Control (MPC) based algorithm is proposed that achieves Regions 1 - 4 control; however, weighting factor selection for MPC influences the performance significantly, and thus, the optimality of the current trajectory is hard to be proved. In the methods proposed by [1][6][7], the basic idea is to adjust i_d with terminal voltage feedback, and the performance of controller depends on PI regulator tuning; here again, the optimality of current trajectory is hard to be guaranteed and one set of parameters cannot fit different machines. In [8][9][10], the control problem is formulated as a constrained optimization problem for which Lagrange Multiplier method is adopted for calculation. Although optimality can be theoretically guaranteed, high computational complexity as shown in the papers impedes these algorithms to be implemented in a high bandwidth PMSM controller.

Therefore, the complexity of PMSM torque control lies in: (1) Controller should be able to generate current trajectory for whole speed range (i.e. Regions 1 - 4); (2) optimality of current reference should be guaranteed so that maximum torque is always generated; (3) computational complexity must be low for high bandwidth controller design. However, none of the algorithms reviewed has achieved the three requirements simultaneously. The algorithm proposed in this paper improves the geometrical linearization approach in [3] and solves for the optimal current trajectory in a different way. With the proposed algorithm, the above mentioned requirements (1) - (3) can be achieved by a single control algorithm.

II. Problem Formulation and Algorithm Description

PMSM torque control can be described by an optimization problem as follows:

$$\begin{aligned} &\min_{(i_d,i_q)} \ \Delta T = \mid T_{cmd} - \frac{3}{2}P \cdot i_q \cdot [\lambda_f + (L_d - L_q) \cdot i_d] \mid \forall \omega_e \\ &s.t. \ \begin{cases} (Ri_d - \omega_e L_q i_q)^2 + [Ri_q + \omega_e (L_d i_d + \lambda_f)]^2 \le U_m^2 \\ i_d^2 + i_q^2 \le I_m^2 \end{cases} \end{aligned} \tag{1}$$

where P, λ_f, L_d, L_q, R and ω_e are machine pole pairs, PM flux linkage, d-q inductances, winding resistance and rotor elec-

trical angular speed, respectively. U_m, I_m are the limitations of inverter. The optimization problem solves for the (i_d, i_q) reference which minimizes torque error for all speed, taking inverter current and voltage limitations as constraints.

Conventional method of using Lagrange Multiplier is quite difficult to obtain closed-form solution for a nonlinear optimization with nonlinear inequality constraints. The proposed algorithm in this paper divides the optimization problem (1) into two sub-optimizations and then solves them sequentially. The first sub-optimization is to solve for a feasible set of a problem that has torque error as the objective function with only voltage as the constraint as given below.

$$\begin{aligned} &\underset{(i_d,i_q)}{min}\ \Delta T = \mid T_{cmd} - \frac{3}{2}P \cdot i_q \cdot [\lambda_f + (L_d - L_q) \cdot i_d] \mid \forall \omega_e \\ &s.t.\ (Ri_d - \omega_e L_q i_q)^2 + [Ri_q + \omega_e(L_d i_d + \lambda_f)]^2 \leq U_m^2 \end{aligned} \tag{2}$$

The feasible set is a portion of the torque hyperbola that satisfies voltage constraint and is denoted by a range of i_d

$$i_{d1} \leq i_d \leq i_{d2} \tag{3}$$

The second sub-optimization has torque error as the objective function and solves for the problem from the feasible set (3) with only current constraint as shown in (4)

$$\begin{aligned} &\underset{(i_d,i_q)}{min}\ \Delta T = \mid T_{cmd} - \frac{3}{2}P \cdot i_q \cdot [\lambda_f + (L_d - L_q) \cdot i_d] \mid \forall \omega_e \\ &s.t.\ \begin{cases} i_{d1} \leq i_d \leq i_{d2} \\ i_d^2 + i_q^2 \leq I_m^2 \end{cases} \end{aligned} \tag{4}$$

The problem is simplified compared with (1) when (2) and (4) are solved sequentially. It will later be shown that solving (2) and (4) by model linearization on (1) can further simplify the optimization process. These two simplifications are at the core of the proposed algorithm, which will be elaborated below based on a typical current trajectory of PMSM (Regions 1 - 4).

III. Geometrical Linearization Approach

Assuming that the winding resistance *R* is small enough, the torque equation is a hyperbola on the $(i_d - i_q)$ plane, while voltage and current constraints are ellipse and circle, respectively. Therefore, the optimization solution of (1) is the (i_d, i_q) pair inside both the voltage ellipse and the current circle, and is closest to hyperbola at the same time. To simplify the problem, Lemmens et al.[3] proposed an algorithm that linearizes torque hyperbola and voltage ellipse on the operating point of PMSM and solves for closed-form solution geometrically. Torque and voltage linearizations are shown in (5).

$$\begin{aligned} dT &= \frac{3}{2}P[(L_d - L_q)i_q \quad \lambda_f + (L_d - L_q)i_d] \begin{bmatrix} di_d \\ di_q \end{bmatrix} \\ d|U| &= \frac{1}{|U|}[RU_d + \omega_e L_d U_q \quad RU_q - \omega_e L_q U_d] \begin{bmatrix} di_d \\ di_q \end{bmatrix} \end{aligned} \tag{5}$$

With linearization, the optimization process changes from $(i_d - i_q)$ plane to $(di_d - di_q)$ plane, on which torque incremental and voltage incremental equations become lines, while current limitation is still kept as a circle with center on $(-i_{dk}, -i_{qk})$ and radius I_m as shown in (6), and (i_{dk}, i_{qk}) is the result of last optimization.

$$(di_d + i_{dk})^2 + (di_q + i_{qk})^2 = I_m^2 \tag{6}$$

The algorithm starts from searching the feasible set of (2) which is the portion on torque hyperbola inside voltage ellipse at the same time. Therefore, intersections between a hyperbola and an ellipse needs to be solved, which is not straight forward however. By torque linearization in (5), (2) is transformed onto $(di_d - di_q)$ plane, where the objective function becomes minimization of the error of required torque change, while constraint becomes the voltage change caused by *d-q* current change as shown by (7) where $dT_{cmd} = T_{cmd} - T_k$ with T_k the torque output of last optimization and dT given by (5).

$$\begin{aligned} &\underset{(di_d,di_q)}{min}\ \Delta dT = \mid dT_{cmd} - dT \mid \\ &s.t.\ [L_q(di_q + i_{qk})]^2 + [L_d(di_d + i_{dk}) + \lambda_f]^2 \leq (\frac{U_m}{\omega_e})^2 \end{aligned} \tag{7}$$

Solving the intersections between a line and an ellipse is still not easy job. By using the variable transformation in[5], voltage ellipse on $(di_d - di_q)$ plane can be further mapped to a circle on a new transformed plane $(di_d^{'} - di_q^{'})$, and the torque change is still a line on the new plane, hence the intersections can finally be obtained for a line and a circle which greatly simplifies the solution. The variable transformations, the transformed voltage limitation and torque incremental equation are shown in (8) and the final simplified optimization on the $(di_d^{'} - di_q^{'})$ plane is shown in (9).

$$\begin{aligned} i_d = i_d^{'} - \frac{\lambda_f}{L_d},\ i_q = i_q^{'}\frac{L_d}{L_q},\ L_d^{'} = \frac{L_d^2}{L_q},\ L_q^{'} = L_d \\ i_d^{'2} + i_q^{'2} = (\frac{U_m}{\omega_e L_d})^2 \end{aligned} \tag{8}$$

$$\begin{aligned} dT^{'} &= \frac{3}{2}P[(L_d^{'} - L_q^{'})i_q^{'} \quad \lambda_f + (L_d^{'} - L_q^{'})i_d^{'}] \begin{bmatrix} di_d^{'} \\ di_q^{'} \end{bmatrix} \\ &\underset{(di_d^{'},di_q^{'})}{min}\ \Delta dT^{'} = \mid dT_{cmd}^{'} - dT^{'} \mid \\ &s.t.\ (di_d^{'} + i_{dk}^{'})^2 + (di_q^{'} + i_{qk}^{'})^2 = (\frac{U_m}{\omega_e L_d})^2 \end{aligned} \tag{9}$$

where $dT_{cmd}^{'} = T_{cmd} - T_k^{'}$ with $T_k^{'}$ the output torque expressed by $i_{dk}^{'}$ and $i_{qk}^{'}$. Once the optimal solution of $(di_d^{'}, di_q^{'})$ is obtained, it needs to be transformed back to $(di_d - di_q)$ plane and the second sub-optimization (4) can be linearized as (10) to obtain the final optimization solution.

$$\begin{aligned} &\underset{(di_d,di_q)}{min}\ \Delta dT = \mid dT_{cmd} - dT \mid \\ &s.t.\ \begin{cases} di_{d1} \leq di_d \leq di_{d2} \\ (di_d + i_{dk})^2 + (di_q + i_{qk})^2 \leq I_m^2 \end{cases} \end{aligned} \tag{10}$$

A typical PMSM current trajectory on $(i_d - i_q)$ plane over the whole speed range is shown in Fig.1. A geometrical

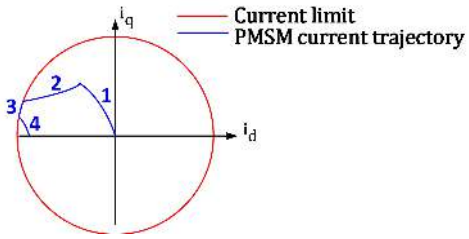

Fig. 1. Typical current trajectory of PMSM over whole speed range.

optimization process of each Region is adopted to solve (9) and (10) which will be elaborated below.

A. Region 1

Region 1 is MTPA operation at low speed. As discussed before, the solution of (9) is the portion of torque change line that is inside the voltage change circle on $(di_d^{'} - di_q^{'})$ plane, as shown in Fig. 2(a). Once the feasible set is obtained and converted back to $(di_d - di_q)$ plane, it is still part of torque line but with a different range. If the required torque change is within the current limit (Fig. 2(b)), the MTPA point is easily obtained by finding the point in the feasible set which has the shortest distance to the current circle center. If the required torque change is larger than the current limit (Fig. 2(c)), the optimal solution is the point on the current circle that has shortest distance to the torque line.

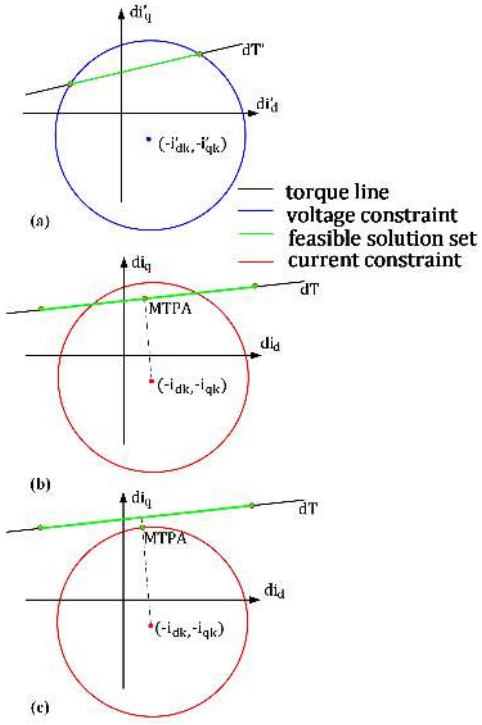

Fig. 2. Geometrical optimization process for Region 1.

B. Region 2

Region 2 is when MTPA operation not feasible but the required torque can still be generated. The feasible set will first be obtained as in Region 1. In Region 2, the MTPA point will not lie inside the feasible set and in this case, the point in the feasible set that has the shortest distance to the current circle center is chosen as the optimal solution (green dot closer to circle center). The process is demonstrated in Fig. 3.

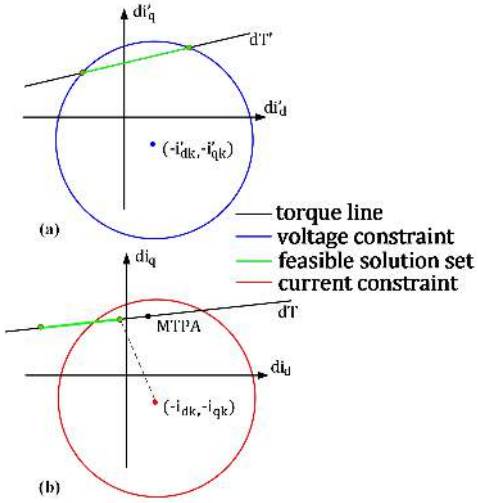

Fig. 3. Geometrical optimization process for Region 2.

C. Region 3

Region 3 is when PMSM enters flux weakening operation and the output torque begins to drop. In Region 3, the feasible set is totally out of the current circle (Fig. 4(b)) and the motor has to operate under both current and voltage limitations. In this region, the current circle will be maintained while the voltage ellipse will be linearized based on (5), and the optimal solution is the intersection between the line and the circle (Fig. 4(c)).

D. Region 4

In this region, the PMSM operates with MTPV and the torque line does not have intersections with voltage circle as it is shrinking. In this case, the only feasible point is the one on the voltage circle closest to torque line (green dot in Fig. 5 (a)). After converting back to $(di_d - di_q)$ plane, the feasible point will lie inside the current circle, which is taken as the solution in this region (green dot in Fig. 5(b)).

Appendix in [3] provides an algorithm to find the optimum solution with a line and a circle. Once the optimal value for (di_d, di_q) is obtained, they need to be converted to absolute current reference by $i_{dq(k+1)} = i_{dq(k)} + di_{dq}$, and a current regulator, such as PI regulator can be used to apply the current reference.

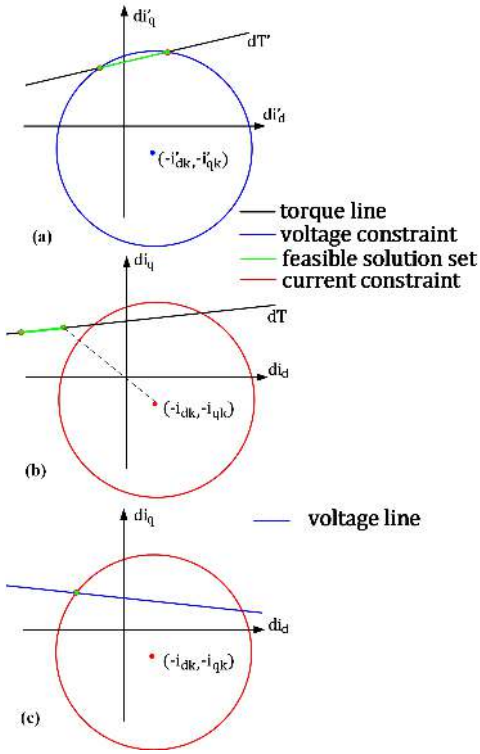

Fig. 4. Geometrical optimization process for Region 3.

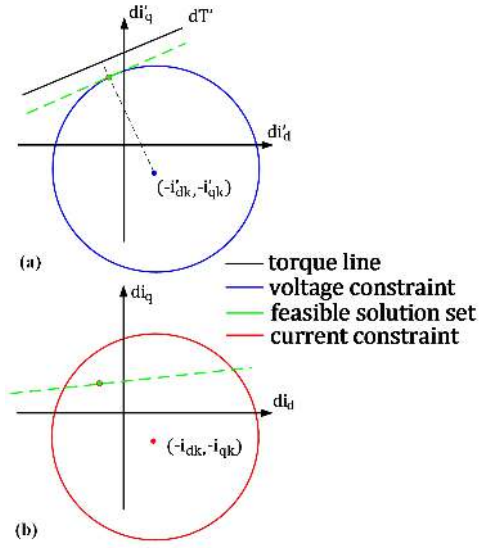

Fig. 5. Geometrical optimization process for Region 4.

IV. Simulation Analysis

The simulation is conducted with a dyno setup where there is a load machine to control the shaft speed, and the PMSM is controlled under torque mode. The parameters used for the simulation are given in Table I.

A. Current Trajectory Test

The test conditions of the simulation are listed in Table II. Fig. 6 shows speed, torque and mechanical power output of the PMSM. The figure shows that the PMSM can generate the required torque below base speed, while beyond base speed, the PMSM enters flux-weakening region. The output power of the machine shows the transition from constant torque to constant power operation. Fig. 7 shows the current trajectory

TABLE I
Parameters of the PMSM under test

Parameters	Value
# of pole pairs	4
d-axis inductance L_d	80uH
q-axis inductance L_q	175uH
Flux linkage λ_f	0.036 vs
Stator resistance R	0.00525Ω (25°C)
Switching frequency	10 kHz
I_{max}	700A
DC bus	200V

TABLE II
Test conditions of Simulation A to E

	T_{cmd}(Nm)	Speed(rpm)
Simulation A	172	0 - 12,000
Simulation B	350	0 - 12,000
Simulation C	172	varying
Simulation D	varying	6,000
Simulation E	±172	±1500

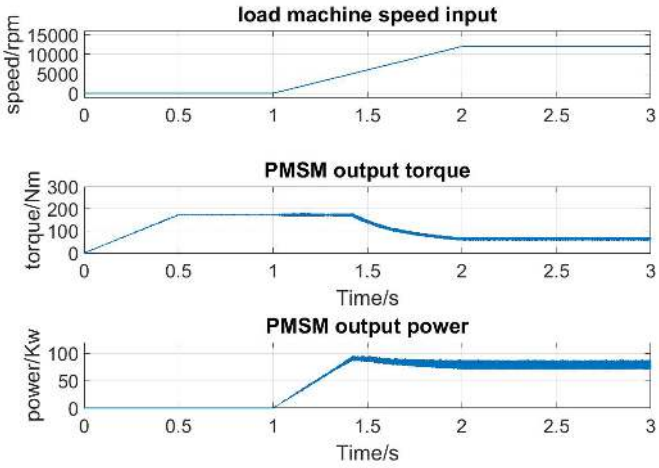

Fig. 6. Speed, torque and mechanical power output of the PMSM.

transition from Region 1 to Region 4 as discussed before. In Fig. 8, two speed-torque envelope curves are compared. The intrinsic capability (red curve) is obtained by solving the original nonlinear optimization (1) with MATLAB function *fmincon()* under the same configuration as the simulation; the blue curve is the torque-speed envelope obtained following the proposed algorithm. The result verifies that the proposed algorithm has a good accuracy for solving the original non-

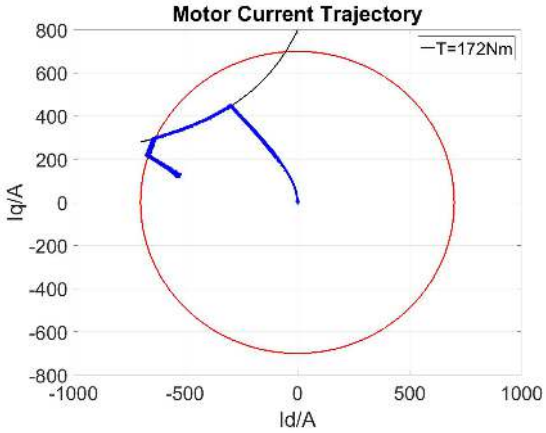

Fig. 7. Current trajectory.

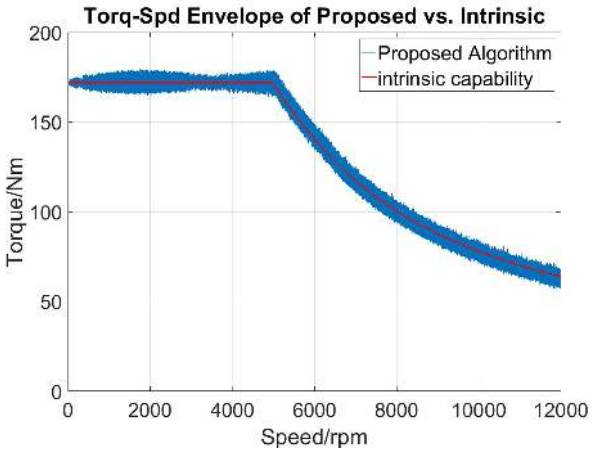

Fig. 8. Comparison between speed-torque envelope obtained by *fmincon()* and algorithm proposed.

linear optimization problem. In contrast, an algorithm that generates sub-optimal current trajectory will have either lower base speed or faster output torque drop or violations on inverter voltage and current.

B. Operating with Voltage/Current Limitations

The simulation conditions are listed in Table II. In this simulation, the torque command (350Nm) is higher than the maximum torque that the PMSM can output for the given current limit (255Nm). Therefore, the PMSM will reach both maximum current and voltage limits during the operation. Fig. 9 shows the current trajectory in this simulation, since torque command is larger than the maximum value possible, the output torque is limited. Fig. 10 shows the PMSM operating within voltage and current constraints for the entire operating speed range. The current limit is I_{m}=700A, and voltage limitation is U_{m}= 115V which is the maximum phase voltage applicable by SVPWM (Space Vector Pulse Width Modulation). Fig. 11 shows the torque-speed envelope of the PMSM in this situation, compared with Fig. 8, for a higher output torque, the PMSM will operate with a lower base speed.

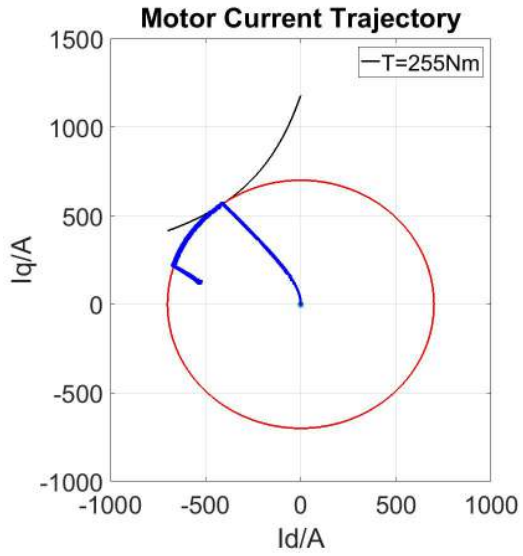

Fig. 9. Current trajectory.

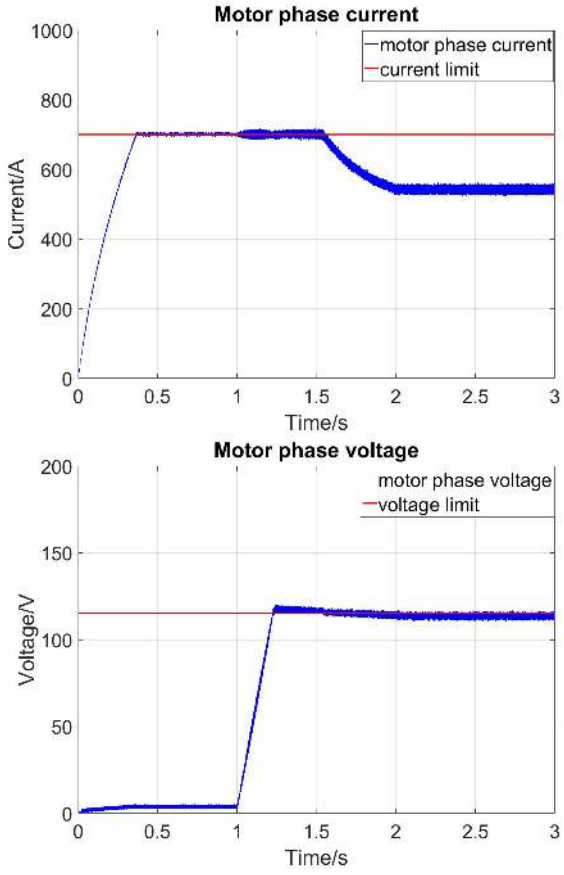

Fig. 10. Motor phase current and voltage maintained within the limitations for the whole speed range.

C. Dynamic Speed

The test conditions of this simulation are shown in Table II for the purpose of verifying if the algorithm is able to solve for the right current command under changing slope and value

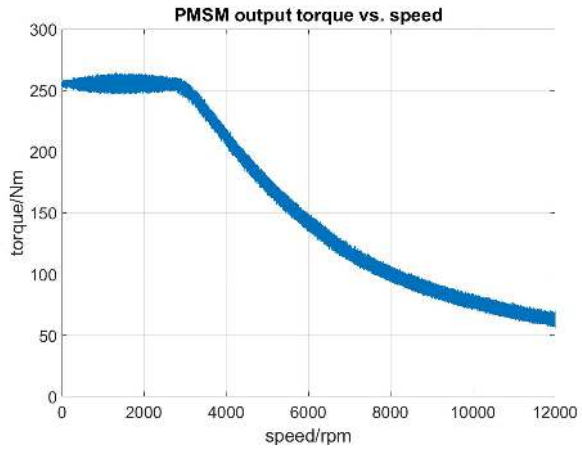

Fig. 11. Torque-speed envelope of the PMSM.

of the speed reference. Fig. 12 shows the speed and torque output of the PMSM. Having a constant torque command and a varying speed, the machine operates in flux weakening region at high speed with a reduced torque output, and follows torque command in the low speed range.

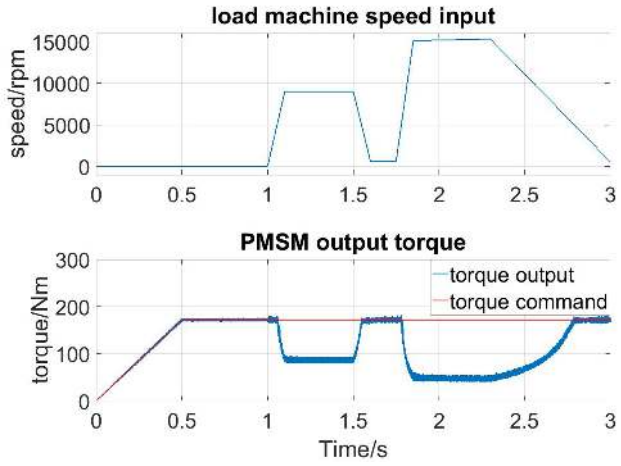

Fig. 12. Constant torque dynamic speed test.

D. Dynamic Torque

The test conditions of the simulation are listed in Table II. In this test, the motor speed is kept constant, while the torque command is dynamically changed to test if the algorithm can solve for the correct solution. Fig. 13 shows the simulation results where the maximum torque output at 6000 rpm is about 143 Nm; below this torque, the PMSM can follow the ramp and step changes of torque command, and has constrained torque output by inverter current and voltage limitation, which is not shown in the simulation since it is impractical.

E. Four Quadrant Operation

This test is conducted to verify if the algorithm can work for all the four quadrants. Test condition is listed in Table II,

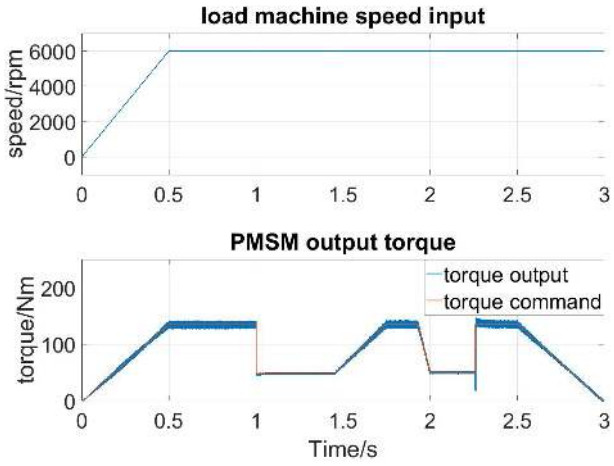

Fig. 13. Constant speed dynamic torque test.

where motor will operate for positive and negtive torque output with forward rotation and positive and negative torque output with reverse rotation. Fig.14 shows the simulation result which verifies that the PMSM operates in all the quadrants.

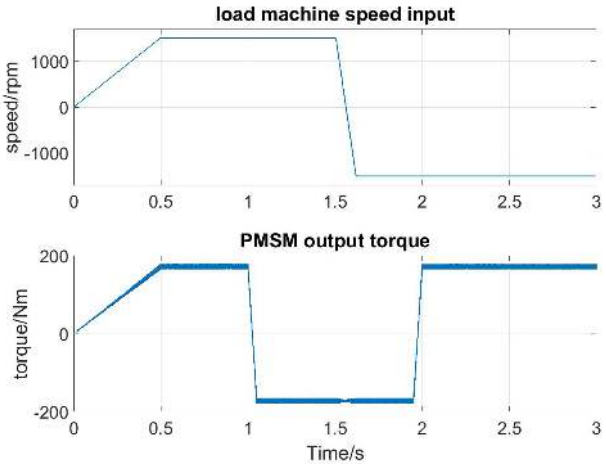

Fig. 14. Four quadrants operation for PMSM.

F. Finite Speed Drive

The previous simulations are all conducted with current limit (700A) larger than the motor characteristic current ($\frac{\lambda_f}{L_d} = 450$A), which makes an infinite speed drive. This simulation tests if the algorithm also works for finite speed drive which has current limit smaller than the motor characteristic current. The test condition is shown in Table III. Fig. 15 shows speed, torque and output power of the PMSM. For the finite speed drive, output torque and power will drop fast during flux weakening region and to zero at the maximum speed that the motor can reach. Fig.16 shows the current trajectory of finite speed drive operation, where MTPV control is not possible and current will move along the current limit circle all the way down till $i_q = 0$.

TABLE III
TEST CONDITIONS OF SIMULATION E

	Current limit(A)	T_{cmd}(Nm)	Speed(rpm)
Simulation F	200	172	0 - 14,000

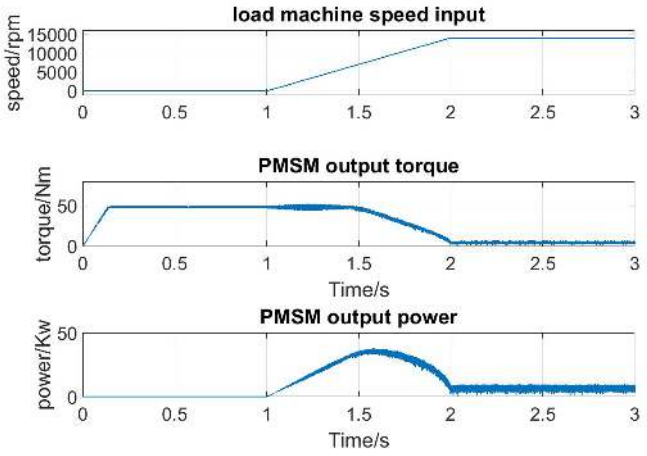

Fig. 15. Speed, torque and power of the finite speed drive PMSM.

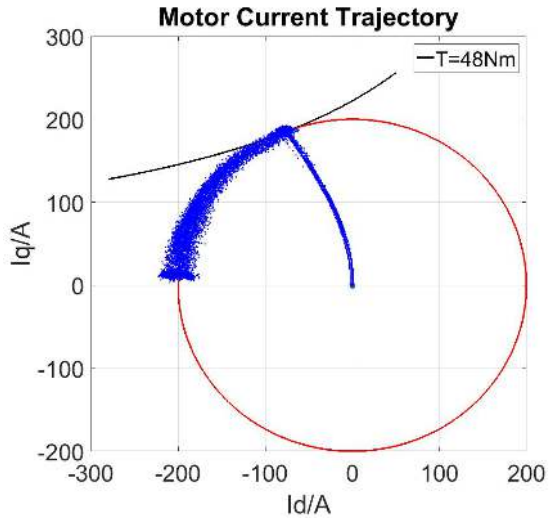

Fig. 16. Current trajectory of the finite speed drive PMSM.

V. CONCLUSION

The nonlinear optimization for PMSM torque control with inverter current and voltage as constraints has been addressed in the presented algorithm by simplifying the problem into two sub-optimization problems. Instead of applying Lagrange Multiplier, linearization of the sub-optimizations is adopted and a geometrical method of solving the linearized optimizations is then proposed to deal with the calculation complexity. Simulation results show that the algorithm is able to generate current reference over the whole speed range and the solution accuracy is remarkable compared with solving the original nonlinear optimization problem. Since each of the two sub-optimization problems is formulated as solving the intersection between a line and a circle, the computation complexity is quite low also. In this regard, the three requirements of PMSM torque controller design described in the introduction can be met simultaneously by the algorithm proposed in this paper. Future work will be implementing the algorithm on a lab PMSM dyno. The key of applying the algorithm is an accurate machine model. For this purpose, a 3-D look up table has been experimentally made for L_d and L_q.

REFERENCES

[1] G. Gallegos-Lopez, F. S. Gunawan and J. E. Walters, "Optimum torque control of permanent-magnet AC Machines in the field-weakened region", IEEE Transactions on Industry Applications, vol. 41, no. 4, pp. 1020-1028, July-Aug. 2005.

[2] S. Morimoto, Y. Takeda, T. Hirasa and K. Taniguchi, "Expansion of operating limits for permanent magnet motor by current vector control considering inverter capacity", IEEE Transactions on Industry Applications, vol. 26, no. 5, pp. 866-871, Sep/Oct 1990.

[3] J. Lemmens, P. Vanassche and J. Driesen, "PMSM Drive Current and Voltage Limiting as a Constraint Optimal Control Problem", IEEE Journal of Emerging and Selected Topics in Power Electronics, vol. 3, no. 2, pp. 326-338, June 2015.

[4] M. Preindl and S. Bolognani, "Model Predictive Direct Torque Control With Finite Control Set for PMSM Drive Systems, Part 1: Maximum Torque Per Ampere Operation", IEEE Transactions on Industrial Informatics, vol. 9, no. 4, pp. 1912-1921, Nov. 2013.

[5] M. Preindl and S. Bolognani, "Model Predictive Direct Torque Control With Finite Control Set for PMSM Drive Systems, Part 2: Field Weakening Operation", IEEE Transactions on Industrial Informatics, vol. 9, no. 2, pp. 648-657, May 2013.

[6] H. Liu, Z. Q. Zhu, E. Mohamed, Y. Fu and X. Qi, "Flux-Weakening Control of Nonsalient Pole PMSM Having Large Winding Inductance, Accounting for Resistive Voltage Drop and Inverter Nonlinearities" IEEE Transactions on Power Electronics, vol. 27, no. 2, pp. 942-952, Feb. 2012.

[7] P. Y. Lin, W. T. Lee, S. W. Chen, J. C. Hwang and Y. S. Lai, "Infinite speed drives control with MTPA and MTPV for interior permanent magnet synchronous motor", IECON 2014 - 40th Annual Conference of the IEEE Industrial Electronics Society, Dallas, TX, 2014, pp. 668-674.

[8] Y. Jeong, S. Sul, S. Hiti and K. M. Rahman, "Online Minimum-Copper-Loss Control of an Interior Permanent-Magnet Synchronous Machine for Automotive Applications", IEEE Transactions on Industry Applications, vol. 42, no. 5, pp. 1222-1229, Sept.-Oct. 2006.

[9] S. Y. Jung, J. Hong and K. Nam, "Current Minimizing Torque Control of the IPMSM Using Ferraris Method", IEEE Transactions on Power Electronics, vol. 28, no. 12, pp. 5603-5617, Dec. 2013.

[10] J. Lee, K. Nam, S. Choi and S. Kwon, "Loss-Minimizing Control of PMSM With the Use of Polynomial Approximations", IEEE Transactions on Power Electronics, vol. 24, no. 4, pp. 1071-1082, April 2009.